RSC Advances

PAPER

View Article Online
View Journal | View Issue

Cite this: *RSC Adv.*, 2024, **14**, 2453

Experimental and *in silico* insights: interaction of dimethyl sulphoxide with 1-hexyl-2-methyl imidazolium bromide/1-octyl-2-methyl imidazolium bromide at different temperatures

Itishree Panda,[a] Bikash Ranjan Behera,[a] Debasmita Jena,[a] Santosh Kumar Behera,*[b] Sangram Keshari Samal *[c] and Sanghamitra Pradhan *[a]

Ionic liquids have gained attention as 'designer solvents' since they offer a broad spectrum of properties that can be tuned by altering the constituent ions. In this work, 1-alkyl-2-methyl imidazolium-based ionic liquids with two different alkyl chains (alkyl = hexyl and octyl) have been synthesized and characterized. Since the binary mixture of ionic liquids with molecular solvents can give rise to striking physicochemical properties, the interaction of the synthesized room temperature ionic liquids, 1-hexyl-2-methyl imidazolium bromide [HMIM][Br]/1-octyl-2-methyl imidazolium bromide [OMIM][Br] with DMSO has been examined through density and specific conductance at T = (303.15, 308.15, 313.15 and 318.15) K under atmospheric pressure. The obtained molar volume and excess molar volume are fitted to the Redlich–Kister polynomial equation, and the standard deviation is noted. The positive excess molar volume at elevated temperatures indicates volume expansion due to the mutual loss of dipolar association and differences in the sizes and shapes of the constituent molecules. To have a better understanding of the reactivity and efficacy of 1-hexyl-2-methyl imidazolium bromide and 1-octyl-2-methyl imidazolium bromide with DMSO, the Becke, 3-parameter, Lee–Yang–Parr (B3LYP) correlation function of density functional theory (DFT) has been used. The ORCA Program version 4.0 calculates the highest occupied molecular orbital (HOMO) and lowest unoccupied molecular orbital (LUMO) energy. The effective reactivities of both the compounds that showed an energy band gap (ΔE), *i.e.*, the difference between E_{LUMO} and E_{HOMO}, are 7.147 and 8.037 kcal mol^{-1}.

Received 31st October 2023
Accepted 3rd January 2024

DOI: 10.1039/d3ra07417j

rsc.li/rsc-advances

Introduction

Solvents are a broad category of chemicals that can be diluted, dissolved, or dispersed by other substances.[1] To produce homogeneous conditions, they facilitate the diffusion of reactants and catalysts. They also store and transmit the thermal energy required for chemical transformations, stabilize transition states, and stop undesired side reactions through dilution. However, common solvents used historically have undetected limitations. Green solvents have been introduced to help reduce the harmful effects of toxic solvents on the environment.[2] High vapor pressure, flammability, toxicity, and air pollution are disadvantages of traditional solvents.[3,4] In several applications, green solvents developed by scientists have outperformed traditional ones. Supercritical fluids, supercritical water, and ionic liquids are alternatives that fall under the "green solvents'' category.[5]

Ionic liquids (ILs), often called ionic melt, liquid electrolytes, ionic fluids, or fused salts, are a class of substances entirely made of ions and capable of liquidity at temperatures below 100 °C.[6,7] Unlike partially ionizable liquids like water/salt solutions and molecular liquids like dichloromethane or hexane, which contain molecules, ILs only contain cations and anions. The generally recognized definition states that these salts have a low vapor pressure and stay liquid below 100 °C.[8,9] ILs are non-flammable and non-volatile substances, making them deemed environmentally beneficial substances. They provide improved reaction speeds, enabling a decrease in solvent amounts during different technological processes, resulting in cost savings and reducing waste risk. ILs can dissolve various organic, inorganic, and polymeric materials over a broad and wide temperature range. They are very viscous, non-flammable, moderately non-ionizing, and non-explosive compounds. ILs are also excellent solvents and have biocatalytic potential. They are also becoming

[a]*Department of Chemistry, Institute of Technical Education and Research (FET), Siksha 'O' Anusandhan, deemed to be University, Khandagiri Square, Bhubaneswar, 751030, Odisha, India*

[b]*Department of Biotechnology, National Institute of Pharmaceutical Education and Research, Ahmedabad, Gujarat 382355, India*

[c]*Laboratory of Biomaterials and Regenerative Medicine for Advanced Therapies, ICMR-Regional Medical Research Center, Bhubaneswar – 751 023, Odisha, India. E-mail: sanghamitrapradhan@soa.ac.in*

more popular as substitute lubricants. Ionic liquids have attracted the attention of scientists due to their wide range of applications in various fields.[10,11] Xu *et al.* have examined the efficiency of 1-octyl-3-methylimidazolium bromide as shale inhibitor. The hydration inhibition ability was investigated through soaking test and hot-rolling dispersion experiment. The inhibition ability of the ionic liquid was analyzed by FT-IR, XRD, TGA and surface tension measurements and the results exhibit the hydration inhibition ability was superior in comparison to other commonly used inhibitors. This was possible because 1-octyl-3-methylimidazolium bromide could easily be adsorbed onto sodium montmorillonite through electrostatic interaction and due to intercalation, water molecules present inside was ejected.[12] This finding was supported by the observations of Luo *et al.* and Yang *et al.*[13,14] The role of imidazolium based ILs in the electrochemical CO_2 reduction reaction has also been explored. The ILs were diluted in acetonitrile to reduce the viscosity and it was observed that the anionic part of the imidazolium salts influenced the solubility of CO_2 and the conductivity of the solution.[15] Likewise, Li *et al.* have investigated on the carboxylate functionalized zeolitic imidazolate framework that enables the catalytic N-formylation utilizing ambient CO_2. The presence of imidazole carboxylate species activates hydrosilane and CO_2 and stimulates amine to take part in the formylation reaction. This indeed augments the catalyst capture and exchange capacity toward ambient CO_2.[16]

Imidazolium-based ILs have received much attention and reporting even though different cation and counter-anion combinations can be used in ILs. The nitrogen-rich heteroatom compound-based ILs have a low melting point, good chemical stability, and excellent ionization performance.[17] Because of the stable positive charge in the aromatic ring, which serves as an adaptable cation framework for the ILs, using imidazolium as a cation structure is a fascinating molecular strategy. The imidazolium ring typically includes two N atoms connected by the methylene group. As a result, the imidazole ring's two nitrogen atoms are classified as N1 (amino nitrogen) donors and N3 (imino nitrogen) acceptors, respectively.[18] The imidazole ring is quaternized with organic substituents, particularly alkyl, aryl, and tertiary nitrogen (N3), to produce imidazolium-based ILs with a permanent positive charge. By doing so, the imidazole ring can take and donate protons during substitution processes. Additionally, secondary amine (N1) undergoes various reactions that support its amphoteric behaviors (accepts and donates protons) and adjustable imidazolium characteristics. As a result, imidazolium-based ILs have a wide range of practical uses, including as catalysts,[19] sensors,[20] adsorption,[21,22] and biomass pre-treatment.[23] Due to their almost nonexistent vapor pressure and ionic makeup, ILs can be helpful in various applications.[24,25] They have significantly impacted the chemical industry due to their perceived status as "designer" or alternative "green" solvents. The ILs can be solvated to a different extent by the solvents due to the presence of various types of interactions such as ionic, hydrogen bonds, π–π, and van der Waals forces. Specifically in non-aqueous solutions, ionic interactions are more dominant due to the partial association of oppositely charged ions to form ion pairs. So, solvation is one of the critical factors in determining the rate of physicochemical processes in solution. Chu and coworkers have demonstrated 2-substituted imidazolium IL as a solvent for the Baylis–Hillman reaction (2-methyl imidazole). It has been shown that 2-methyl-substituted positions are rationally acidic and mainly synthesized by alkylation reactions.[26] Shekaari *et al.* have reported on density, speed of sound and electrical conductance of 1-hexyl-3-methylimidazolium bromide in aqueous medium at different temperatures. The derived properties like apparent molar volume and isentropic compressibility have been calculated for different temperatures using the density and speed of sound. The calculated thermophysical properties reflect that interaction between IL and water decreases with increase in temperature.[27] On the other hand, Dash *et al.* have examined the thermophysical measurements of aqueous solution of 1-hexyl-3-methyl-imidazolium bromide at 298.15 K and 0.1 MPa. The negative excess molar volume at this temperature indicates the compactness of the solution resulting from attractive interaction between the unlike components due to hydrogen bonding.[28] The density, viscosity, and conductivity of 1-butyl-3-methylimidazolium bromide in water, methanol, ethanol, and acetonitrile have been measured at room temperature. The density decreases with rise in temperature and conductivity showed increasing trend.[29] Recently, the solubility of ILs in polar solvents like dimethyl sulphoxide (DMSO), dimethylacetamide (DMA), dimethylformamide (DMF) have gained adequate attention due to their increasing dissolving rates and low costs at different temperatures compared to pure ILs.[30,31] It has been reported that the solution of 1-butyl-3-methylimidazolium acetate in DMSO, DMF and DMA can efficiently dissolve cellulose at room temperature. DMSO has been considered as the most appropriate co-solvent for ILs for dissolving cellulose.[32] Therefore binary mixtures of ionic liquids with DMSO are increasingly used for varied sectors.[33–35] Amphiphilic molecule like DMSO contains a hydrophilic sulfoxide group with two hydrophobic methyl groups. It is endowed with two vital properties; it is soluble in water and possesses the potential to dissolve varied lipophilic compounds. The hydrophilic groups mainly form hydrogen bonds, and hydrophobic moieties tend to self-aggregate. To understand the usefulness of the solvent, the knowledge of the molecular interaction mechanisms, particularly the structure-making and breaking associations and interstitial accommodation, is essential to understand the ion–ion and ion–solvent interactions that exist in the binary mixtures.

In this perspective, in the first section, we initially present the thermophysical properties of the two synthesized 2-methylimidazolium-based ionic liquids and the mixture of ILs with DMSO.[36] At atmospheric pressure, density and specific conductance were recorded for both systems in the range of 303.15 to 318.15 K. Using the density measurements, the molar volumes of the binary mixtures at different temperatures were calculated. The excess values were calculated and fitted to the Redlich–Kister polynomial. To add novelty to this work and gain more insight into the orientation of the molecules after the

Table 1 Lists of chemicals used in the study

Chemicals	Purity	Molecular formula	Molecular mass (g mol^{-1})	Density (g cm^{-3})	CAS no.	Source
2-Methylimidazole	99%	$C_4H_6N_2$	82.10	1.09	693-98-1	Sigma-Aldrich
1-Bromohexane	99%	$CH_3(CH_2)_5Br$	165.08	1.18	111-25-1	Loba Chemie
1-Bromooctane	98%	$CH_3(CH_2)_7Br$	193.12	1.112	111-83-1	Loba Chemie
Chloroform	≥99%	$CHCl_3$	119.38	1.474	67-66-3	Merck
Acetone	≥99%	CH_3COCH_3	58.08	0.784	67-64-1	Merck
DMSO	≥99%	$(CH_3)_2SO$	78.13	1.101	67-68-5	Merck

interaction, quantum chemical calculations applied in modeling simulation studies have been performed.

Experimental

Materials

The chemicals used in the study are listed in Table 1. All the chemicals were used as such without further purification.

Methods

Synthesis. In a round bottom flask fitted, 0.01 mol of 2-methylimidazole was taken, and to it 0.02 mol of bromo alkanes (bromo hexane and bromo octane) were added with chloroform. The round bottom flask was fitted with a condenser and stirred for 6 h at 70 °C. The temperature was maintained to get the best result. The solution was left undisturbed overnight, and the obtained liquid was brownish-yellow viscous[37] (Fig. 1). The IR studies were taken for the obtained IL.

Characterisation and thermophysical measurements

The FTIR spectra were recorded using Shimadzu IR-Spectrometer (FTIR 8201) within the 4000–400 cm^{-1}. For thermophysical measurements, the required quantity of the synthesized ILs; 1-hexyl-2-methyl imidazolium bromide [HMIM][Br] and 1-octyl-2-methyl imidazolium bromide [OMIM][Br] were mixed with DMSO based on volume with a calculated precision of $\pm 1 \times 10^{-4}$ in mole fraction. The binary mixtures' mole fraction was calculated using the density and volume values. The density was recorded at $T = 303.15$, 308.15, 313.15 and 318.15 K with the help of a pycnometer and Citizen digital balance (CY 320C). It was calibrated using double distilled water. A Japanese conductivity meter made by Horiba Laqua called the F74 was used to evaluate the conductance of the binary mixtures and pure components. The uncertainties were estimated to be 0.1% for concentration and 1% for conductivity, respectively.

Data analysis

The molar volumes (V_{12}) of the binary mixture of 1-hexyl-2methylimidazolium bromide [HMIM][Br]/1-octyl-2methylimidazolium bromide [OMIM][Br] with DMSO have been calculated using the density (ρ_{12}) data recorded at $T =$ (303.15, 308.15, 313.15 and 318.15) K, given in eqn (1)

$$V_{12} = (X_1M_1 + X_2M_2)/\rho_{12} \quad (1)$$

where X_1, X_2, M_1, and M_2 represent the mole fraction and molecular mass of DMSO and [HMIM][Br]/[OMIM][Br] respectively and ρ_{12} is the density of the binary mixture of ILs and DMSO.

The excess molar volume V_{12}^E is calculated using eqn (2)

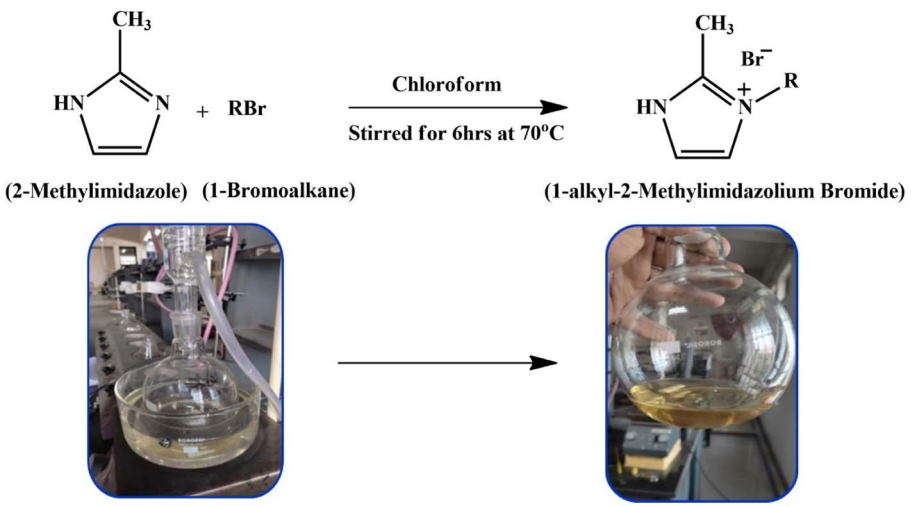

Fig. 1 Synthesis of 1-alkyl-2-methyl imidazolium bromide (where R = hexyl and octyl).

$$V_{12}^{E} = V_{12} - (V_1X_1 + V_2X_2) \quad (2)$$

where V_1 and V_2 are the molar volumes of the DMSO and [HMIM][Br]/[OMIM][Br] respectively.

The values of the excess properties are correlated by using the Redlich–Kister polynomial using eqn (3)

$$V_{12}^{E} = X_1X_2\sum_{i=0}^{m} B_i(2X_2 - 1)^i \quad (3)$$

where, B_i is the fitting coefficient and m represents the order of the polynomial equation.

The standard deviations, $\sigma(V_{12}^{E})$ have been reported using the following expression (4)

$$\sigma(V_{12}^{E}) = [\sum(V_{12,exp}^{E} - V_{12,cal}^{E})^2/(n - m)]^{1/2} \quad (4)$$

where, n symbolizes the experimental data points and m is the number of coefficients respectively.

In silico analysis

Retrieval of compounds. The structures of (a) 1-hexyl-2-methyl imidazolium bromide (b) 1-octyl-2-methyl imidazolium bromide, and (c) dimethyl sulfoxide was drawn using ChemDraw20.0 software. The structures were converted to.pdb format, using Chen3D 20.0 software, the preferred format for various *in silico* analyses.

In silico combinatorial chemistry

Combinatorial chemistry is the sum of repetitive and covalent coupling of different "building blocks" to represent a spectrum of structurally different molecules called as chemical library. In the current arena, computational tools play a pivotal role in Combinatorial chemistry through combinatorial drugs, which is the preferred aegis of the pharmaceutical sector. It is well known that solvent and thermal effect play a crucial role in understanding the properties of a drug metabolism. Taking together the above concerns, the compounds [HMIM][Br] and [OMIM][Br] interacted with the solvent dimethyl sulfoxide through an *In silico* approach (Schrödinger Release 2022-4: Maestro, Schrödinger, LLC, New York, NY, 2022).

Density functional theory (DFT) for quantum chemical calculation

Quantum computation studies were performed with the help of density functional theory (DFT) to investigate the reactivity and efficiency of the compounds. The reactivity of [HMIM][Br] and [OMIM][Br] were analyzed using the Becke, 3-parameter, Lee–Yang–Parr (B3LYP) correlation function of DFT. The DFT analysis was performed using the highest occupied molecular orbital (HOMO) and lowest unoccupied molecular orbital (LUMO) energy. The ORCA Program version 4.0 was used for calculation of energy of orbitals. The electronic energy, frontier HOMOs, LUMOs, gap energy, and dipole moment were measured for the potential drugs. The following eqn (5) was used for calculation of DFT.

$$E = \min_n\left\{\int V_{nuclei}(\vec{r})n(\vec{r})\mathrm{d}^3\vec{r} + F[n(\vec{r})]\right\} \quad (5)$$

where, $\{V_{nuclei} + nr\}n \equiv$ trial density and $F \equiv$ universal functional.

Molecular dynamics (MD) simulations

Molecular dynamics (MD) is a sophisticated computational tool for envisaging and analyzing the physical movements of atoms and molecules in macromolecular structure-to-functions.[36] The mode of binding, the specificity of the substrate, and the dynamic behaviour can be clearly explained. The atoms and molecules are allowed to interact in a set time. This clearly illustrates the system's dynamic "evolution".[38] The MD protocol includes minimization, heating, equilibration, and production.[39] The OPLS4 force field was used for minimization, and topology and atomic coordinates were obtained automatically, followed by the addition of ILs to the DMSO solvent model orthorhombic box (15 × 15 × 10 Å).[40] The Particle Mesh Ewald (PME) boundary condition has been used to ensure that no solute atoms occurred within 10 Å distance of the border. The entire system was simulated at 303.15 and 318.15 K for 100 ns using the NPT ensemble, and the structural alterations and dynamic behaviour were investigated using root mean square deviation (RMSD) and root mean square fluctuation (RMSF) graphs. The RMSF method is used to find the flexible region.[41]

Results and discussion

FTIR analysis

To validate the synthesis of [HMIM][Br] and [OMIM][Br], an active group investigation of ILs using FT-IR data was used (Fig. 2). Several discernible peaks provided evidence for an imidazolium ring, including N–H stretching at 3397.96 cm^{-1}, C=C at 1601.51 cm^{-1}, and C=N at 1617.98 cm^{-1}. Peaks obtained at 1378.85 cm^{-1}, 3063.37 cm^{-1}, and 1117.55 cm^{-1} supported the existence of an imidazolium ring. Aliphatic C–H stretch signals were also discovered at 2928.35 cm^{-1}, pointing

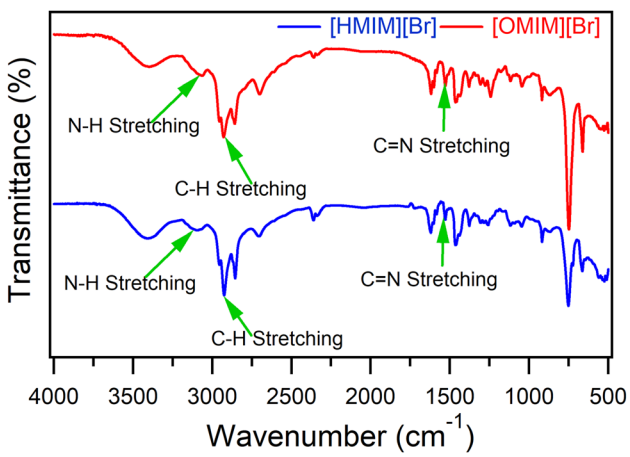

Fig. 2 FTIR spectrum of pure [HMIM][Br] (in blue) and [OMIM][Br] (in red).

Table 2 Density of pure [HMIM][Br] and [OMIM][Br][a]

Temperature (K)	Density (g cm^{-3})	
	[HMIM][Br]	[OMIM][Br]
303.15	1.2621	1.2074
308.15	1.2602	1.2072
313.15	1.2591	1.2068
318.15	1.2583	1.2064

[a] Standard uncertainties (0.68 level of confidence) for $T = 0.001$ K, $U(c)\rho = 0.0001$ g cm^{-3}.

to the presence of alkyl chain groups.[42–44] Numerous earlier studies revealed that the absence of the C–Br stretching absorbance band in the IR spectra for the absorption of single-element anions Br was caused by the synthesis of the imidazolium salt and the lack of bond vibration.[45–47]

Density measurements

The density of pure [HMIM][Br] and [OMIM][Br] has been measured at T = 303.15, 308.15, 313.15, and 318.15 K and presented in Table 2.

The densities of the binary mixture of the ILs with DMSO recorded in the temperature range of 303.15–318.15 K at 5 K intervals have been represented in (Fig. 3). From the plots, it is evident that the density of the binary mixture of ILs with DMSO increases with the increase in mole fractions of [HMIM][Br] and [OMIM][Br]. This is because the densities of ILs are more than the solvent DMSO. But with the temperature rise, it is observed that the density of the binary mixture decreases with an increase in the mole fraction of the ILs.

Molar volume

The derived properties, such as molar volumes, were calculated using density values (ρ_{12}) of the binary mixtures of [HMIM][Br]/[OMIM][Br] in DMSO at different temperatures. As the density decreases with an increase in the mole fraction of [HMIM][Br] and [OMIM][Br], the molar volume of the binary mixture increases. This behavior is justified because density and volume are inversely related.[48] With the temperature rise, the molar volume displays an increasing trend due to the mutual loss of dipolar association and the constituent molecules' differences in shape and size (Table 3).

Table 3 Representation of molar volumes (V_{12}) of binary mixture of [HMIM][Br]/[OMIM][Br] in DMSO at different temperatures[a]

	V_{12} (cm^3 mol^{-1})			
X_2	303.15 K	308.15 K	313.15 K	318.15 K
[HMIM][Br]				
0.267	106.041	106.601	107.269	107.587
0.327	113.280	114.215	115.049	115.438
0.422	124.765	126.883	127.533	127.860
0.594	145.568	148.475	149.595	149.972
0.700	158.248	161.502	162.571	162.841
0.900	182.986	184.748	185.343	185.642
[OMIM][Br]				
0.236	109.078	109.655	110.924	111.221
0.292	117.611	118.442	119.793	120.217
0.383	131.908	132.706	134.214	134.685
0.557	158.914	160.024	161.649	162.348
0.700	181.684	182.482	183.770	184.319
0.900	212.337	213.223	214.117	214.477

[a] Standard uncertainties (0.68 level of confidence) for $T = 0.001$ K, $U(c)\rho = 0.0001$ g cm^{-3}.

Excess properties

The mixture's molecular environment is altered by adding more of a component, dramatically changing the forces between different molecules, and affecting the thermodynamic characteristics of the binary liquid system.[49] The easiest way to describe the departure from ideality in a liquid mixture is through the excess thermodynamic properties. The experimental density data of the binary mixtures were used to compute the excess molar volume values (V_{12}^{E}). The standard deviation values and coefficients that were obtained after the experimental data were fitted into the Redlich–Kister

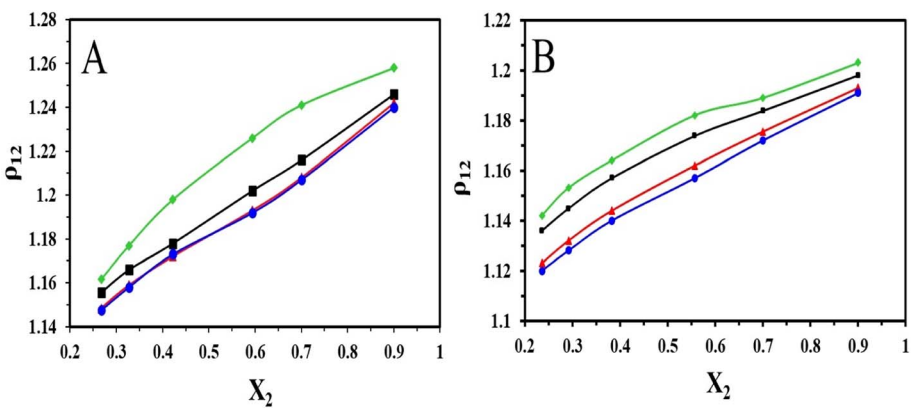

Fig. 3 Plot of variation of density with different mole fractions of (A) [HMIM][Br] and (B) [OMIM][Br] at T = (◆303.15, ■308.15, ▲313.15 and ●318.15) K.

Table 4 List of coefficients and standard deviation values of [HMIM][Br] and [OMIM][Br] at $T = 303.15$, 308.15, 313.15 and 318.15 K

Temp. (K)	B_0	B_1	B_2	B_3	σ
[HMIM][Br]					
303.15	0.889	−7.150	0.541	0.018	0.017
308.15	10.007	6.444	−5.45	0.011	0.002
313.15	12.728	−9.492	−4.320	−0.051	0.094
318.15	12.186	9.997	−5.183	0.095	0.116
[OMIM][Br]					
303.15	−11.543	6.886	−2.925	0.001	0.181
308.15	3.632	3.483	4.752	9.807	0.466
313.15	8.893	4.207	7.121	−0.047	0.490
318.15	10.624	5.902	5.968	−0.064	0.401

polynomial are displayed in Table 4. The excess characteristics are estimated using the Redlich–Kister fitting coefficients. Fig. 4 represents the excess molar volume for the binary mixture of [HMIM][Br] and DMSO at $T = 303.15$, 308.15 K, 313.15 K, and 318.15 K. At 303.15 K, the excess tends to be positive, and after that, a negative trend follows. But at higher temperatures, there is a positive trend at all mole fractions of [HMIM][Br]. Two competing causes have led to this. Volume expansion is carried on by mutual loss of dipolar association and differences in the sizes and shapes of the constituent molecules. Dipole-induced interactions between polar and dissimilar molecules bring on volume contraction. The experiment results indicate that the latter effect predominated in the binary mixture, supporting the idea that structural factors cause mixtures to expand relative to pure components. The variation in V_{12}^{E} for binary combinations is shown in (Fig. 5) based on the mole fraction of [OMIM][Br]. In comparison to [HMIM][Br], the V_{12}^{E} values are negative at all mole fractions of [OMIM][Br], indicating the indirect influence of the H-bond formed by the neighboring functional group S═O with hydrogen present in the alkyl chain. This observation was in coherence with the findings of Dash *et al.* where negative excess volume was noted at 298.15 K for solution of 1-hexyl-3-methylimidazolium bromide in water due to hydrogen bonding that resulted in compactness of the system.[28]

In this study, the V_{12}^{E} values are affected by several variables, including geometric, chemical, and physical aspects. It is clear from the detailed examination that the molecular interaction between the [HMIM][Br]/[OMIM][Br] + DMSO is more dominant in case [OMIM][Br] at 303.15 K due to greater chain length of the alkyl group. Due to the absence of a dipolar connection at high temperatures, V_{12}^{E} values suggest that the interactions between the binary mixture's constituents are not selective.

Conductivity measurements

The measurement of the conductivity of ILs gives information about the ionic interactions in the liquid mixtures. Due to the viscous nature of ionic liquids, the conductivity tends to remain low. The conductivity of pure IL is influenced by the presence of cosolvent. The increase or decrease of conductivity relies on the nature of the solvent and the extent of dissociation of IL into ions.[50] The conductivity of neat [HMIM][Br] and [OMIM][Br] at $T = 303.15$, 308.15, 313.15, and 318.15 K have been recorded and presented in Table 5.

Fig. 6 represent the variation of specific conductivity of the binary mixtures of [HMIM][Br]/[OMIM][Br] and DMSO. It is observed that at low mole fraction of ILs, the specific

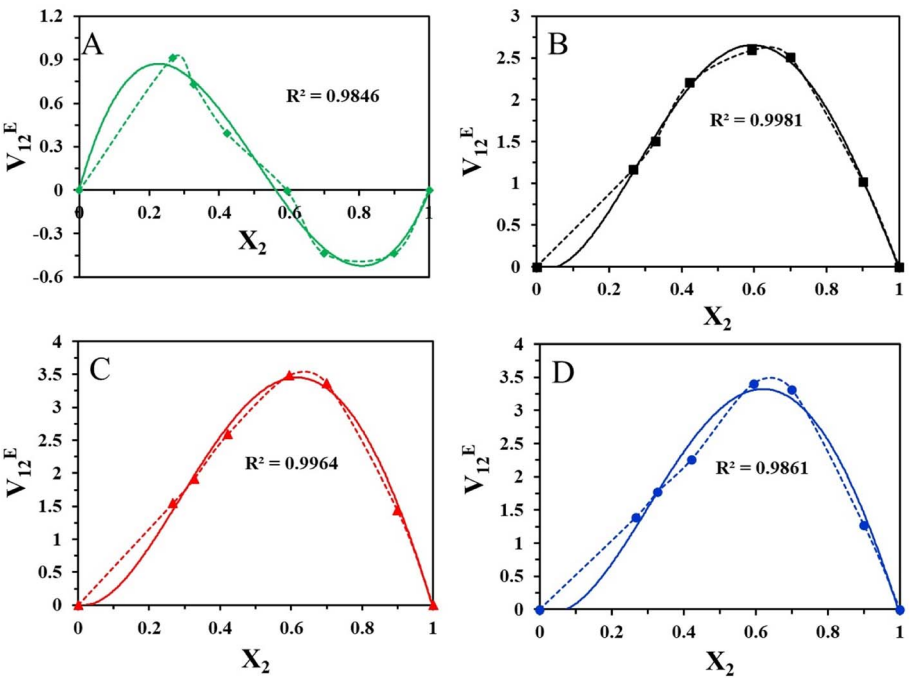

Fig. 4 Representation of V_{12}^{E} of [HMIM][Br] in DMSO at $T = (\blacklozenge 303.15$ (A), ■ 308.15 (B), ▲ 313.15 (C) and ● 318.15 (D)) K. The solid lines represent the Redlich–Kister correlations and dotted lines denote the experimental values.

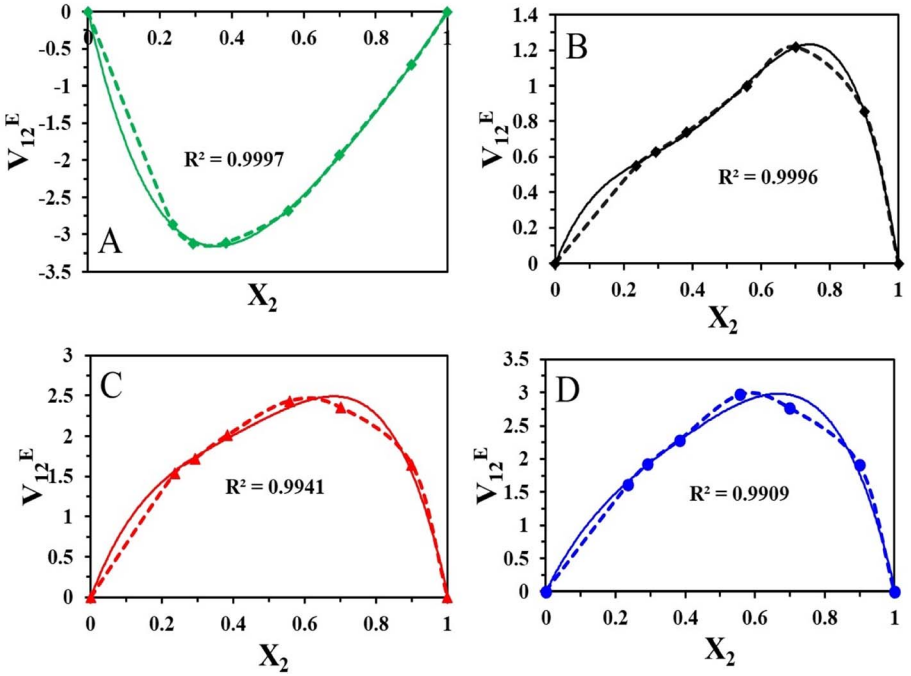

Fig. 5 Representation of V_{12}^E of [OMIM][Br] in DMSO at T = (◆303.15 (A), ■308.15 (B), ▲313.15 (C) and ●318.15 (D)) K. The solid lines represent the Redlich–Kister correlations and dotted lines denote the experimental values.

conductivity value is high but gradually decreases as the concentration increases. This clearly indicates that smaller ions can move more easily than the larger ions. On the other hand, it is detected that as the temperature increases the conductivity of [HMIM]/[OMIM] in DMSO increases. This observation is well supported by the expansion in volume and positive excess molar volumes. This finding showed similar trend as reported for 1-butyl-3-methylimidazolium bromide in water where the conductivity increased with rise in temperature.[29]

Table 5 Representation of specific conductivity of pure [HMIM][Br] and [OMIM][Br] at different temperatures

Temperatures in K	Specific conductivity (κ), S cm^{-1}	
	[HMIM][Br]	[OMIM][Br]
303.15 K	1.013	1.141
308.15 K	1.159	1.205
313.15 K	1.216	1.425
318.15 K	1.330	1.625

Quantum chemical calculation

Quantum chemical calculations applied in modelling simulation studies can be used for investigating frontier molecular characteristics. Considering the importance of the structure and reactivity of compounds, we carried out DFT simulations for [HMIM][Br] and [OMIM][Br] using ORCA Programme (version 4.0) to understand its geometry and orientation (Table 6).

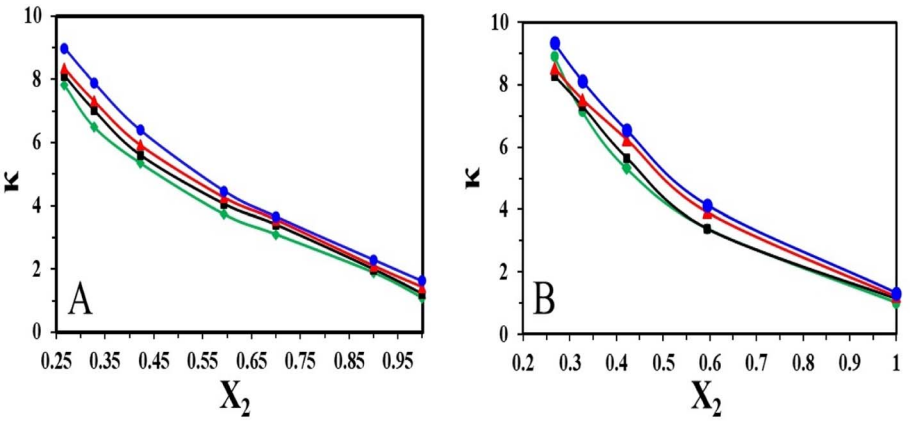

Fig. 6 Plot of specific conductivity of (A) [HMIM][Br] and (B) [OMIM][Br] in DMSO at T = (◆303.15, ■308.15, ▲313.15 and ●318.15) K.

Table 6 Electronic energy, energy in atomic unit of highest occupied molecular orbital (HOMO), lowest unoccupied molecular orbital (LUMO), gap energy and dipole moment of the compounds DFT

Pubchem compound ID	Compound	Electronic energy (eV)	E_{LUMO} (kcal mol^{-1})	E_{HOMO} (kcal mol^{-1})	GAP energy (ΔE) (kcal mol^{-1})	Dipole moment (Debye)
ChemDraw	[HMIM][Br]	−83547.243	1.349	−5.798	7.147	25.60293
ChemDraw	[OMIM][Br]	−85670.505	1.778	−6.259	8.037	21.97936

The effective reactivity for both the compounds which showed band energy gap (ΔE), *i.e.* the difference between E_{LUMO} and E_{HOMO}, was 7.147 and 8.037 kcal mol^{-1} (Fig. 7A–D).

The lower the gap energy, the higher the reactivity. [HMIM][Br] displayed the most remarkable reactivity compared to [OMIM][Br] based on its lowest band energy gap, which was calculated to be 7.147 kcal mol^{-1}.

Trajectory analysis of MD simulations

In the current investigation, we employed the MD simulations for two compounds immersed in DMSO under different temperatures. The interaction studies were Holo1: [HMIM][Br] interacting with DMSO at 303.15 K, Holo2: [HMIM][Br] interacting at 318.15 K, Holo3: [OMIM][Br] interacting with DMSO at 303.15 K and Holo4: [OMIM][Br] interacting with DMSO at 318.15 K using Desmond suit (Schrödinger Release 2022-4: Maestro, Schrödinger, LLC, New York, NY, 2022) in order to understand the dynamic behaviour, mode of binding and inhibitor specificity in all the four systems. A 100 ns MD simulation was used to assess structural rearrangements as well as the stability of such combinations. The RMSD profile of the backbone atoms, at 100 ns, was used to determine the dynamic stability of all the systems (Holo1–Holo4) (Fig. 8A–D).

The backbone RMSD graph of Holo1: [HMIM][Br] interacting with DMSO at 303.15 K, depicted a consistent instability throughout the MD simulation time compared to Holo2: [HMIM][Br] interacting with DMSO at 318.15 K, which revealed a comparative stable trajectory after 70 ns of MD simulation, during 100 ns of simulation time frame. In Holo1 state the RMSD reflected value between ∼0.1 to ∼1.8 Å, from 0 to 100 ns of MD simulations whereas Holo2 state depicted the RMSD value between ∼0.3 to ∼1.8 Å. The RMSD graph of Holo1 revealed slightly higher deviations compared to Holo2. This depicts that the temperature may play a vital role in the interaction of compound [HMIM][Br] with DMSO solvent and can assist in stabilizing and destabilizing through changing its conformation compared to Holo1. Similarly, RMSD of Holo3: [OMIM][Br] interacting with DMSO at 303.15 K revealed a stable trajectory after 90 ns of MD simulation, during 100 ns of simulation time frame compared to Holo4. In the Holo3 state, the RMSD reflected a value between ∼0.4 to ∼2.0 Å, from 90 to 100 ns of MD simulations, whereas the Holo4 state depicted the RMSD value between ∼0.8 to ∼1.6 Å from 30 to 50 ns but after 50 ns of MDS there were deviations. The RMSD graph of Holo3 revealed slightly higher deviations compared to Holo4. This depicts that the temperature may play a key role in interaction

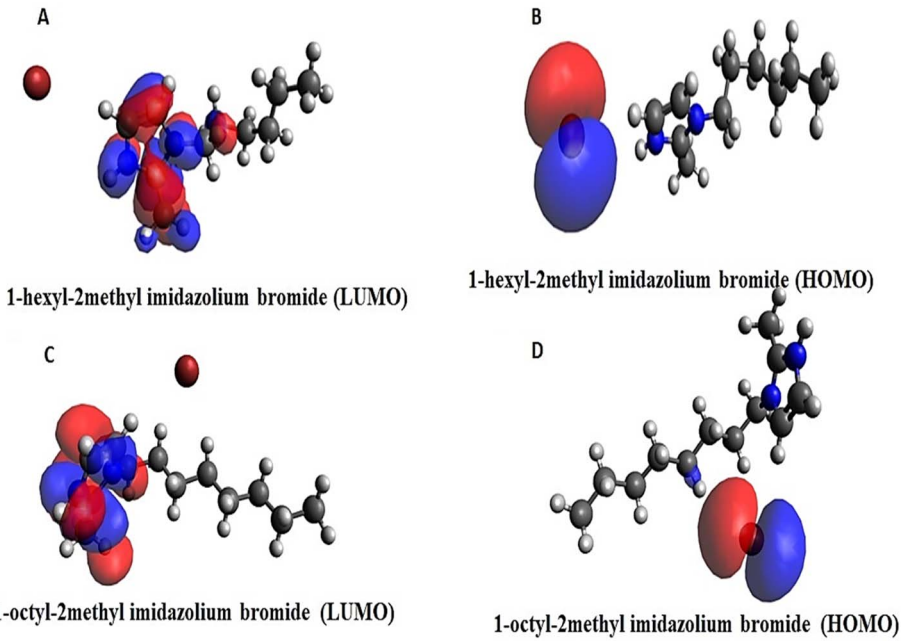

Fig. 7 LUMO and HOMO plots of [HMIM][Br] (A and B) and [OMIM][Br] (C and D) which exhibited higher reactivity. Red colour indicates the positive electron density and the negative electron density in represented in blue colour.

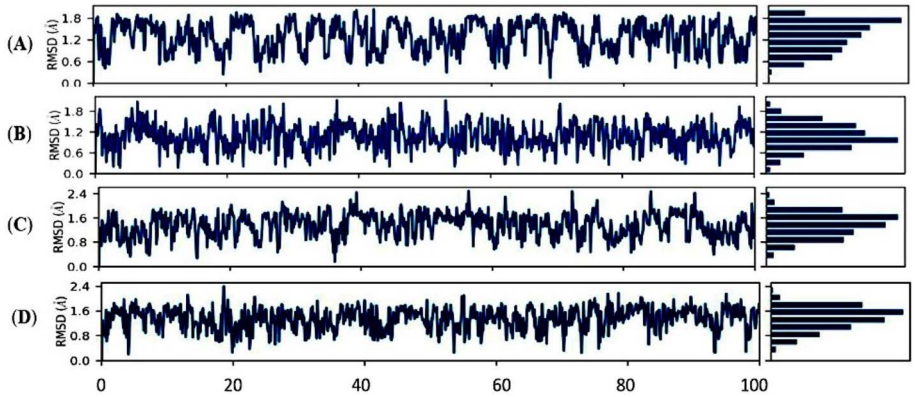

Fig. 8 Conformational RMSD stability of Holo states throughout 100 nanoseconds (ns) time period of MDS. (A) Backbone-RMSD of [HMIM][Br]–DMSO at 303.15 K. (B) Backbone-RMSD of [HMIM][Br]–DMSO at 318.15 K. (C) Backbone-RMSD of [OMIM][Br]–DMSO at 303.15 K. (D) Backbone-RMSD of [OMIM][Br]–DMSO at 318.15 K.

of compound [OMIM][Br] interacting with DMSO solvent at 318.15 K can assist in stabilizing and destabilizing through changing its conformation when compared to Holo3.

The RMSD finding was further corroborated by RMSF to monitor the fluctuation of atoms. The mobility of different atoms was observed in both the states through RMSF plots (Fig. 9A–D).

Overall, the Holo3 and Holo4 state showed more fluctuations than the Holo1 and Holo2 state which are depicted in peaks of the RMSF graph, demonstrating the simulation's constrained

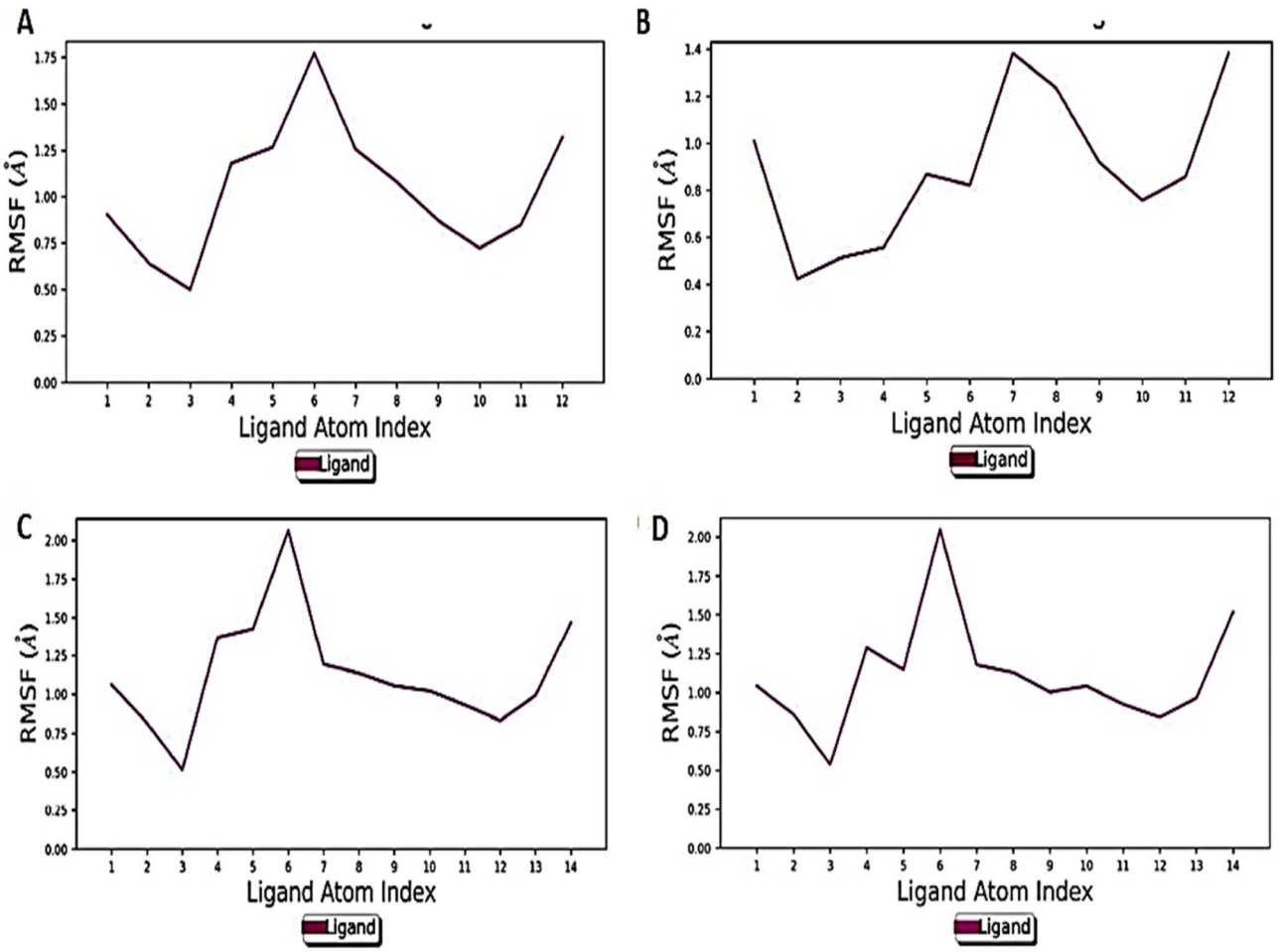

Fig. 9 Conformational stability of Apo and Holo states recorded throughout 100 nanoseconds of MDS. Cα-RMSF profile of (A) [HMIM][Br]–DMSO at 303.15 K, (B) [HMIM]–DMSO at 318.15 K, (C) [OMIM][Br]–DMSO at 303.15 K, (D) [OMIM][Br]–DMSO at 318.15 K.

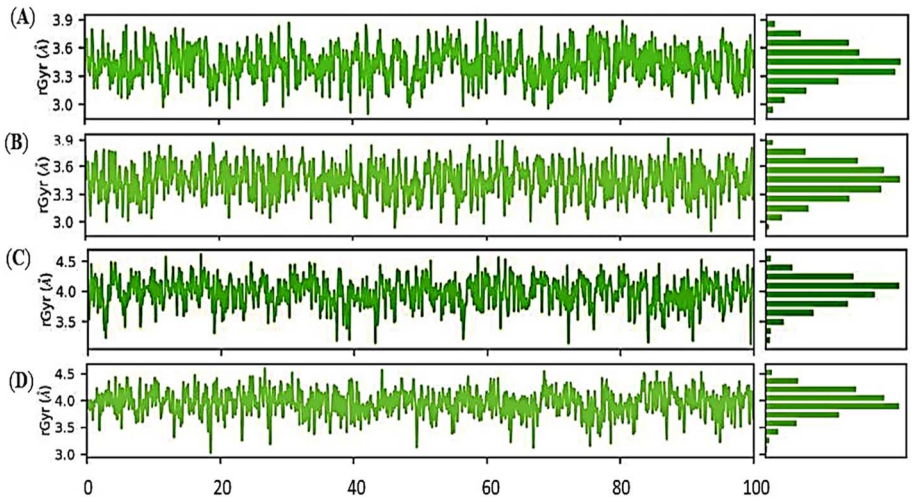

Fig. 10 MD simulations of 100 nanoseconds for solvent accessible surface analysis (SASA); (A) [HMIM][Br]–DMSO at 303.15 K, (B) [HMIM][Br]–DMSO at 318.15 K, (C) [OMIM][Br]–DMSO at 303.15 K, (D) [OMIM][Br]–DMSO at 318.15 K.

motions. The overall compactness for all the states during the simulation of 100 ns was explained using properties such as radius of gyration (*r*Gyr), as shown in (Fig. 10A–D).

The radius of gyration (*r*Gyr) equals its principal moment of inertia. The fluctuation graphs of *r*Gyr *vs.* simulation duration show that Holo1 showed decrease in gyration during 90 to 100 ns of MD simulations. In case of Holo2 the *r*Gyr remains constantly fluctuated over the simulation procedure. The 1-hexyl-2-methyl imidazolium bromide interacting with DMSO at 303.15 K *r*Gyr variation ranging from ~3.0 to ~3.7 Å during 90 to 100 ns time frame, and ~2.9 to ~3.7 during 90 to 100 ns time frame in Holo2. Holo3 depicted *r*Gyr values ~3.1 to ~4.4 Å throughout the MD simulation time frame. Holo4 depicted *r*Gyr values ~3.2 to ~4.4 Å during 90 to 100 ns time frame. Taking to gather all the *r*Gyr values Holo1 indicated more compact than Holo2 state and other states, representing that the value of *r*Gyr is inversely proportional to compactness and *vice versa*.[51] These consequences of *r*Gyr are well supported by RMSF analysis. The frequency of the interactions between ILs and DMSO is directly proportional to the visible surface area. SASA's illustration (Fig. 11A–D).

Mainly in the Holo states, the available solvent surface was reduced. The findings of SASA revealed that the Holo1: [HMIM][Br] interacting with DMSO at 303.15 K, can alter the hydrophilic and hydrophobic interaction areas, which might potentially affect the orientations. During 55 ns to 75 ns MD simulation, the SASA graph of Holo1 reflected a buried stat represented SASA with ~380 to ~430 Å^2. The Holo2 state represented SASA with ~400 to ~430 Å^2, during 30 to 50 ns of MD simulation time frame. In case of Holo3 and Holo4 the SASA value was ~440 Å^2 to ~480 Å^2 during 50 to 70 ns and ~425 Å^2 to ~480 Å^2 during 60 to 80 ns of time frame. The results of SASA

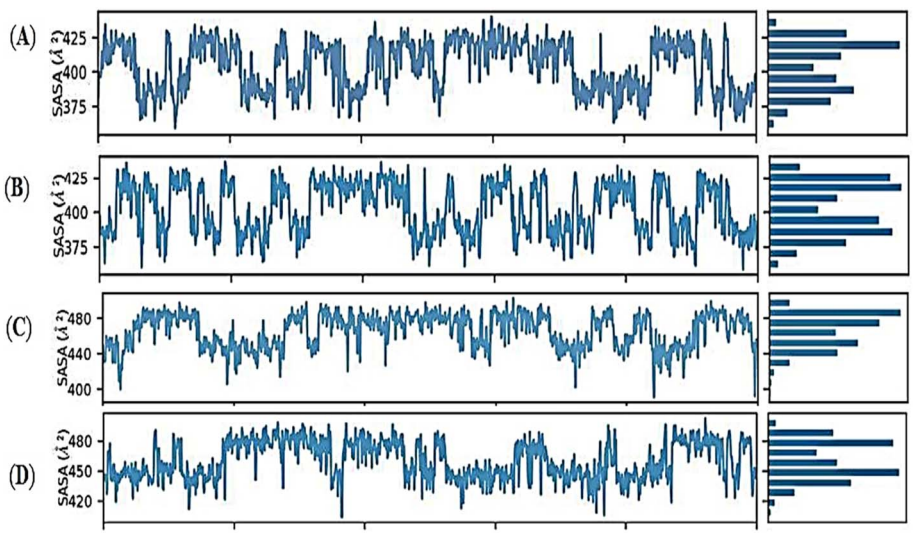

Fig. 11 MD simulations of 100 nanoseconds for solvent accessible surface analysis (SASA); (A) [HMIM][Br]–DMSO at 303.15 K, (B) [HMIM][Br]–DMSO at 318.15 K, (C) [OMIM][Br]–DMSO at 303.15 K, (D) [OMIM][Br]–DMSO at 318.15 K.

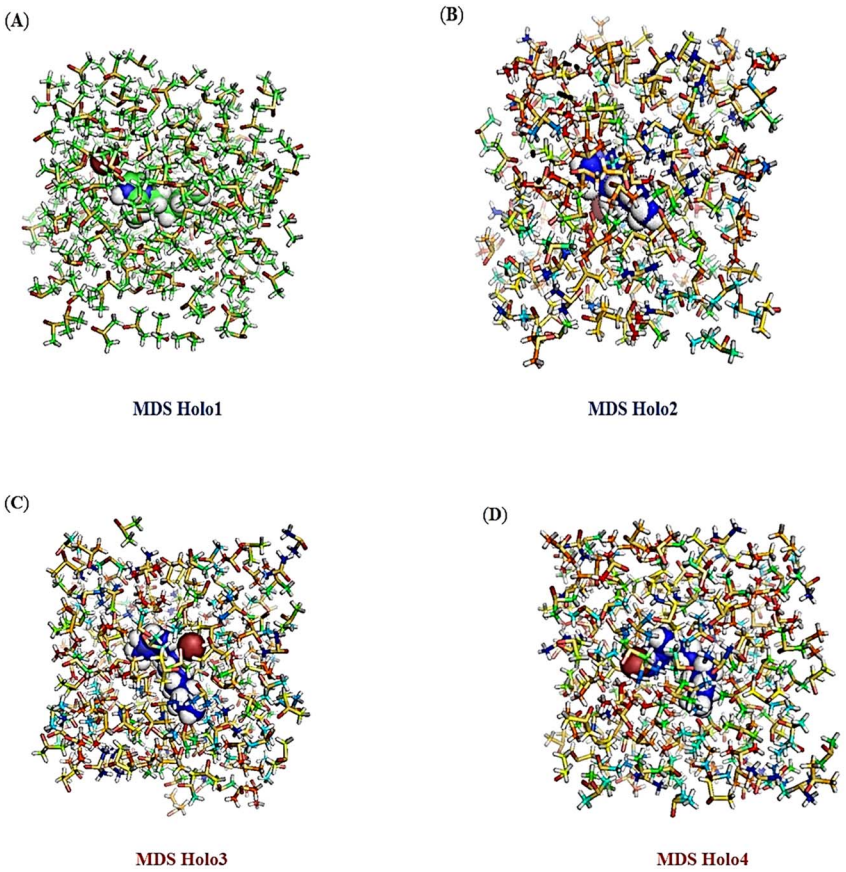

Fig. 12 MDS interaction study. (A) [HMIM][Br]–DMSO at 303.15 K, (B) [HMIM][Br]–DMSO at 318.15 K, (C) [OMIM][Br]–DMSO at 303.15 K, (D) [OMIM][Br]–DMSO at 318.15 K. The images were generated by PyMol tool.

depict that temperature plays a key role in orientation change during the interaction of compound and solvent. This may be the reason for getting different time frames for buried regions in other Holo states. This suggests that the atoms of Holo states may shift from the accessible to the buried region may produce an orientational change.

Post MDS analysis

During MD simulations, the intra and inter molecular atomic bonds of the Holo states were plotted using Schrödinger Release 2022-4 (Fig. 12A–D). Simulation of all the Holo states revealed variable bonding during the simulation. The post MD simulation analysis of revealed change in the atomic arrangement in Holo states. Compared to Holo1, and Holo3, Holo2 and Holo4 were found to have comparatively more compactness.

Conclusions

Density and conductivity measurements of [HMIM][Br] and [OMIM][Br] in DMSO have been reported at temperatures $T =$ (303.15, 308.15, 313.15 and 318.15) K. The molar volume and excess molar volume evaluated using density data correlated well with the Redlich–Kister polynomial. The parameters indicate that the interaction between [HMIM][Br]/[OMIM][Br] and DMSO decrease with increase in temperature from 303.15 to 318.15 K. This observation was in coherence with similar systems reported in literature. The negative excess molar volume for the binary mixtures at 303.15 K for all mole fractions of [OMIM][Br] indicates the formation of hydrogen bonds between the S=O and alkyl chain. However, there is a loss of dipolar connection between the components as the temperature rises. The conductivity of the ILs increases with temperature indicating non-specific interaction between the ILs and DMSO. The energy difference between the LUMO and HOMO of the systems has been calculated using DFT. The MD simulation studies reveal that temperature play a vital role in orientation change during the interaction of ionic liquids with the solvent. This suggests that the atoms of Holo states may shift from accessible to buried region and may result in orientational change. Overall, both experimental and computational results will undeniably provide appreciated and exceptional knowledge on molecular interactions between ILs and DMSO which have been the spotlight of chemical research in the last decade.

Author contributions

Conceptualization: Sanghamitra Pradhan. Data Curation: Itishree Panda, Bikash Ranjan Behera, Debasmita Jena, Santosh Kumar Behera, Sangram Keshari Samal, Sanghamitra Pradhan. Funding acquisition: Sanghamitra Pradhan, Sangram Keshari Samal, Santosh Kumar Behera. Investigation: Itishree Panda,

Bikash Ranjan Behera, Debasmita Jena, Santosh Kumar Behera, Sangram Keshari Samal, Sanghamitra Pradhan. Software: Sanghamitra Pradhan, Sangram Keshari Samal, Santosh Kumar Behera. Supervision: Sanghamitra Pradhan. Visualization, writing – original draft, writing – review & editing: Itishree Panda, Bikash Ranjan Behera, Debasmita Jena, Santosh Kumar Behera, Sangram Keshari Samal, Sanghamitra Pradhan.

Conflicts of interest

The authors have no conflicts of interest to declare.

Acknowledgements

Ms. Itishree Panda acknowledges the Siksha 'O' Anusandhan Deemed to be University for providing Ph.D. fellowship. Dr Sangram Keshari Samal highly acknowledges the Ramanujan fellowship (SB/S2/RJN-038/2016) of the Department of Science and Technology, and Ramalingaswami Re-entry fellowship (Ref: D.O. No. BT/HRD/35/02/2006) of Department of Biotechnology, Government of India. The authors also thank the Indian Council of Medical Research-Regional Medical Research Centre, Bhubaneswar for providing a scientific platform. The authors also express their deep sense of gratitude to Department of Biotechnology, National Institute of Pharmaceutical Education and Research, Ahmedabad, Gujarat for giving us the chance to use Schrödinger, LLC, New York, NY, 2022 (Schrödinger Release 2022-4: Maestro, Schrödinger, LLC, New York, NY, 2022).

References

1 C. J. Clarke, W.-C. Tu, O. Levers, A. Brohl and J. P. Hallett, Green and sustainabke solvents in chemical processes, *Chem. Rev.*, 2018, **118**, 747–800.
2 M. Petkovic, K. R. Seddon, L. P. N. Rebelo and C. Silva Pereira, Ionic liquids: a pathway to environmental acceptability, *Chem. Soc. Rev.*, 2011, **40**, 1383–1403.
3 M. Espino, M. de los Ángeles Fernández, F. J. V. Gomez and M. F. Silva, Natural designer solvents for greening analytical chemistry, *TrAC, Trends Anal. Chem.*, 2016, **76**, 126–136.
4 Z. Xue, L. Qin, J. Jiang, T. Mu and G. Gao, Thermal. electrochemical and radiolytic stabilities of ionic liquids, *Phys. Chem. Chem. Phys.*, 2018, **20**, 8382–8402.
5 H. Machida, M. Takesue and R. L. Smith, Simultaneous and selective recovery of cellulse and hemicellulose fractions from wheat bran supercritical water hydrolysis, *J. Supercrit. Fluids*, 2011, **60**, 2–15.
6 M. Galiński, A. Lewandowski and I. Stępniak, Ionic liquid as electrolytes, *Electrochim. Acta*, 2006, **51**, 5567–5580.
7 *Ionic Liquids as Green Solvents*, ed. R. D. Rogers and K. R. Seddon, American Chemical Society, Washington, DC, 2003, vol. 856.
8 Z. Lei, B. Chen, Y.-M. Koo and D. R. MacFarlane, Introduction: Ionic liquids, *Chem. Rev.*, 2017, **117**, 6633–6635.
9 J. P. Hallett and T. Welton, Room temperature ionic liquids: solvents for synthesis and catalysis, *Chem. Rev.*, 2011, **111**, 3508–3576.
10 S. K. Singh, S. Banerjee, K. Vanka and P. L. Dhepe, Understanding interactions between lignin and ionic liquids with experimental and theoretical studies during catalytic depolymerization, *Catal. Today*, 2018, **309**, 98–108.
11 P. G. Jessop, Fundamental properties and practical applications of ionic liquids: concluding remarks, *Faraday Discuss.*, 2018, **206**, 587–601.
12 J. Xu, Z. Qiu, X. Zhao, H. Zhong and W. Huang, Study of 1-octyl-3-methylimidazolium bromide for inhibiting shale hydration and dispersion, *J. Pet. Sci. Eng.*, 2019, **177**, 208–214.
13 Z. Luo, L. Wang, P. Yu and Z. Chen, Experimental study on the application of an ionic liquid as shale inhibitor and inhibitive mechanism, *Appl. Clay Sci.*, 2017, **150**, 267–274.
14 L. Yang, G. Jiang, Y. Shi and X. Yang, Application of ionic liquid and polymeric ionic liquid as shale hydration inhibitors, *Energy Fuels*, 2017, **31**, 4.
15 A. Fortunati, F. Risplendi, M. R. Fiorentin, G. Cicero, E. Parisi, M. Castellino, E. Simone, B. Iliev, T. J. S. Schubert, N. Russo and S. Hernandez, Understanding the role of imidazolium-based ionic liquids in the electrochemical CO_2 reduction reaction, *Commun. Chem.*, 2023, **6**, 84.
16 Z. Li, H. Li and S. Yang, Carboxylate-functionalized zeolitic imidazolate framework enables catalytic N-formylation using ambient CO_2, *Adv. Sustainable Syst.*, 2022, **6**, 2100380.
17 S. Pal, A. Mukherjee and P. Ghosh, Imidazolium based ionic liquid-assisted processing of natural biopolymers containing amine/amide functionalities for sustainable fiber production, *Mater. Today Sustain.*, 2021, **14**, 100082.
18 A. Verma, S. Joshi and D. Singh, Imidazole: Having versatile biological activities, *J. Chem.*, 2013, **2013**, 1–12.
19 H. Wan, Z. Wu, W. Chen, G. Guan, Y. Cai, C. Chen, Z. Li and X. Liu, Heterogenization of ionic liquid based on mesoporous material as magnetically recyclable catalyst for biodiesel production, *J. Mol. Catal. A: Chem.*, 2015, **398**, 127–132.
20 R. Gao, D. Wang, J. R. Heflin and T. E. Long, Imidazolium sulfonate containing pentablock copolymer-ionic liquid membranes for electroactive actuators, *J. Mater. Chem.*, 2012, **22**, 13473.
21 S. Kassaye, K. K. Pant and S. Jain, Hydrolysis of cellulosic bamboo biomass into reducing sugars *via* a combined alkaline solution and ionic liquid pretreatment steps, *Renewable Energy*, 2017, **104**, 177–184.
22 Z. Zhao, H. Dong and X. Zhang, The research progress of CO_2 capture with ionic liquids, *Chin. J. Chem. Eng.*, 2012, **20**, 120–129.
23 S. K. Singh and P. L. Dhepe, Novel synthesis of immobilised Bronsted-acidic ionic liquid: application of lignin depolymerization, *ChemistrySelect*, 2018, **3**, 5461–5470.
24 M. Filice, J. M. Guisan and J. M. Palomo, Effect of ionic liquids as additives in the catalytic properties of different immobilized preparations of *Rhizomucor miehei* lipase in

the hydrolysis of peracetylated lactal, *Green Chem.*, 2010, **12**, 1365.
25 K. R. Seddon, A. Stark and M.-J. Torres, Influence of chloride, water, and organic solvents on the physical properties of ionic liquids, *Pure Appl. Chem.*, 2000, **72**, 2275–2287.
26 J.-C. Hsu, Y.-H. Yen and Y.-H. Chu, *Tetrahedron Lett.*, 2004, **45**, 4673–4676.
27 H. Shekaari, Y. Mansoori and R. Sadeghi, Density, speed of sound, and electrical conductance of ionic liquid 1-hexyl-3-methyl-imidazolium bromide in water at different temperatures, *J. Chem. Thermodyn.*, 2008, **40**, 852–859.
28 D. Dash, S. Kumar, C. Mallika and U. K. Mudali, *Thermophysical, Volumetric, and Excess Properties of Aqueous Solutions of 1-Hexyl-3-Methylimidazolium Bromide at 298.15 K and 0.1 MPa*, Hindawi Publishing Corporation, 2013.
29 P. N. Tshibangu, S. N. Ndwandwe and E. D. Dikio, Density, viscosity and conductivity study of 1-butyl-3-methylimidazolium bromide, *Int. J. Electrochem. Sci.*, 2011, **6**, 2201–2213.
30 R. Rinaldi, Instantaneous dissolution of cellulose in organic electrolyte solutions, *Chem. Commun.*, 2011, **47**, 511–513.
31 A. Xu and F. Wang, Carboxylate ionic liquid solvent systems from 2006 to 2020: thermal properties and application in cellulose processing, *Green Chem.*, 2020, **22**, 7622–76664.
32 A. Xu, Y. Wang and R. Liu, Cellulose dissolution in diallylimidazolium methoxyacetate + N-methylpyrrolidinone mixture, *Sci. Rep.*, 2019, **9**, 11518.
33 N.-N. Wang, Q.-G. Zhang, F.-G. Wu, Q.-Z. Li and Z.-W. Yu, Hydrogen bonding interactions between a representative pyridinium based ionic liquid [BuPy][BF_4] and water/Dimethyl sufoxide, *J. Phys. Chem. B*, 2010, **114**, 8689–8700.
34 S. Zhao, X. Tian, Y. Ren, J. Wang, J. Liu and Y. Ren, A theoretical investigation of the interactions between hydroxyl-functionalized ionic liquid and water/methanol/dimethyl sulfoxide, *J. Mol. Model.*, 2016, **22**, 195.
35 G. Rai and A. Kumar, Probing thermal interactions of ionic liquids with dimethyl sulfoxide, *ChemPhysChem*, 2012, **13**, 1927–1933.
36 K. Chen, B. Xu, L. Shen, D. Shen, M. Li and L.-H. Guo, Functions and performance of ionic liquids in enhancing electrocatalytic hydrogen evolution reactions: a comprehensive review, *RSC Adv.*, 2022, **12**, 19452–19469.
37 W. Feng, Y. Lu, Y. Chen, Y. Lu and T. Yang, Thermal stability of imidazolium based ionic liquids investigated by TG and FTIR techniques, *J. Therm. Anal. Calorim.*, 2016, **125**, 143–154.
38 J. D. Durrant and J. A. McCammon, Molecular dynamics simulations and drug discovery, *BMC Biol.*, 2011, **9**, 71.
39 R. Raghu, V. Devaraji, K. Leena, S. D. Riyaz, P. Baby Rani, P. Kumar Naik, P. K. Dubey, D. Velmurugan and M. Vijayalakshmi, Virtual screening and discovery of novel aurora kinase inhibitors, *Curr. Top. Med. Chem.*, 2014, **14**, 2006–2019.
40 D. Shivakumar, J. Williams, Y. Wu, W. Damm, J. Shelley and W. Sherman, Prediction of absolute solvation free energies using molecular dynamics free energy perturbation and the OPLS force field, *J. Chem. Theory Comput.*, 2010, **6**, 1509–1519.
41 I. Aier, P. K. Varadwaj and U. Raj, Structural insights into conformational stability of both wild-type and mutant EZH2 receptor, *Sci. Rep.*, 2016, **6**, 34984.
42 Q. Ge, D. Lou, J. Zeng, C. Pan, S. Wang, W. Zhang, L. Zhang and X. Wang, Structural evolution of imidazolium-based poly(ionic liquid) assemblies during solvent evaporation, *eXPRESS Polym. Lett.*, 2017, **11**, 84–95.
43 B. B. Polesso, R. Duczinski, F. L. Bernard, H. Z. Ferrari, M. da Luz, F. D. Vecchia, S. M. C. de Menezes and S. Einloft, Enhancement of CO_2/N_2 selectivity and CO_2 uptake by tuning concentration and chemical structure of imidazolium based ILs immobilized in mesoporous silica, *Mater. Res.*, 2019, **22**, 84–95.
44 D. Danielewicz, M. Kmiotek and B. Surma-Ślusarska, Properties and fibre characterisation of bleached hemp, birch and pine pulps : a comparison, *Fibres Text. East. Eur.*, 2019, **27**, 118–123.
45 D. F. Montaño, H. Casanova, W. I. Cardona and L. F. Giraldo, Functionalization of monomorillonite with ionic liquids based on 1-alkyl-3-methylimidazolium: Effect of anion and length chain, *Mater. Chem. Phys.*, 2017, **198**, 386–392.
46 G. Ameta, A. K. Pathak, C. Ameta, R. Ameta and P. B. Punjabi, Sonochemical synthesis and characterization of imidazolium based ionic liquids: A green pathway, *J. Mol. Liq.*, 2015, **211**, 934–937.
47 A. Ahmed, Y. Chaker, E. H. Belarbi, O. Abbas, J. N. Chotard, H. B. Abassi, A. N. Van Nhien, M. El Hadri and S. Bresson, XRD and ATR/FTIR investigations of various montmorillonite clays modified by monocationic and dicationic imidazolium ionic liquids, *J. Mol. Struct.*, 2018, **1173**, 653–664.
48 S. Pradhan and S. Mishra, A thermodynamic investigation of solute-solvent interactions through volumetric, ultrasonic, dielectric, refractive and excess properties of binary mixtures of Tri-n-butyl phosphate with dichloro, trichloro and tetrachloromethane at 298.15 K, *J. Mol. Liq.*, 2019, **279**, 561–570.
49 S. Pradhan, S. K. Behera, S. K. Samal, I. Panda, P. K. Sahu and S. Priyadarshini, Interaction between 2-methylimidazole and 1-butanol/1-octanol: Thermophysical and computational studies, *ChemistrySelect*, 2023, **8**(13), e202204931.
50 S. Thawarkar, N. D. Khupse and A. Kumar, Solvent-mediated molar conductivity of protic ionic liquids, *Phys. Chem. Chem. Phys.*, 2015, **17**, 475–482.
51 S. Behera, N. Mahapatra, C. Tripathy and S. Pati, Drug repurposing for identification of potential inhibitors against SARS-CoV-2-spike receptor binding domain: An *in silico* approach, *Indian J. Med. Res.*, 2021, **153**, 132.